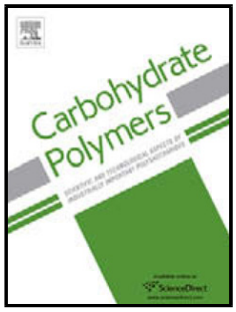

Title: Structure, rheology, and copper-complexation of a hyaluronan-like exopolysaccharide from *Vibrio*

Authors: Manuel Martin-Pastor, Andreia S. Ferreira, Xavier Moppert, Cláudia Nunes, Manuel A. Coimbra, Rui L. Reis, Jean Guezennec, Ramon Novoa-Carballal

PII: S0144-8617(19)30659-9
DOI: https://doi.org/10.1016/j.carbpol.2019.114999
Article Number: 114999

Reference: CARP 114999

To appear in:

Received date: 4 March 2019
Revised date: 14 June 2019
Accepted date: 14 June 2019

Please cite this article as: { https://doi.org/

Structure, rheology, and copper-complexation of a hyaluronan-like exopolysaccharide from *Vibrio*

Manuel Martin-Pastor[a], Andreia S. Ferreira[b], Xavier Moppert[c], Cláudia Nunes[c], Manuel A. Coimbra[b], Rui L. Reis[e,f], Jean Guezennec*[d] and Ramon Novoa-Carballal*[e]

[a] Unidade de Resonancia Magnética, RIAIDT, CACTUS, Campus Vida, Univ. Santiago de Compostela,15782 A Coruña, Spain

[b] QOPNA/LAQV & [c] CICECO, Departamento de Química, Universidade de Aveiro, Campus de Santiago, 3810-193 Aveiro, Portugal

[d] Pacific Biotech BP 140 289 Arue Tahiti (Polynésie Française), France

[e] 3B´s Research Group – Biomaterials, Biodegradables and Biomimetics, University of Minho, Headquarters of the European Institute of Excellence on Tissue Engineering and Regenerative Medicine, AvePark, 4805-017 Barco, Guimarães, Portugal & ICVS/3B's - PT Government Associate Laboratory, Braga/Guimarães, Portugal

[f] The Discoveries Centre for Regenerative and Precision Medicine, Headquarters at University of Minho, Avepark, 4805-017 Barco, Guimarães, Portugal;

e-mail: rnovoausc@yahoo.es,

Highlights

- An exopolysaccharide (EPS) was isolated from bacterial mats in French Polynesia
- The structure repeating unit is →4)-β-D-Glc*p*A-(1→4)-α–D-Gal*p*NAc-(1→3)-β–D-Glc*p*NAc-(1→4)-β-D-Glc*p*A-(1→.
- The main structure is identical to EPS secreted by Vibrio diabolicus
- MO245 has equal ratio of GlcA to N-acetylated sugars and the same glyosidic linkages than HA
- The structural similarity to HA provides MO245 with similar physicochemical properties
- The rheological properties and gel formation with metal ions reveals MO245 potential for biomedical applications.

Abstract

MO245 exopolysaccharide (EPS) was produced in laboratory conditions from *Vibrio* genus microorganism isolated from bacterial mats found in Moorea Island. Its structure consists of a linear tetrasaccharide repeating unit →4)-β-D-Glc*p*A-(1→4)-α-D-Gal*p*NAc-(1→3)-β-D-Glc*p*NAc-(1→4)-β-D-Glc*p*A-(1→ containing covalently-linked 5% of glucose, galactose, and rhamnose, determined by methylation analyses and NMR spectroscopy. The molecular weight, radius of gyration (R_g) and intrinsic viscosity, [η], determined by gel permeation chromatography with light scattering and viscosity detection, were 513±4 kDa (PDI, 1.42±0.01), 6.7±0.3 dl/g and 56±0.3 nm respectively. The chelation of the EPS with copper divalent ions leads to the instantaneous formation

of gels. The structural similitude proposed, based in an equal ratio of GlcA to N-acetylated sugars and in the same type of glyosidic linkages present in the repeating unit (alternated 1→3 and 1→4 linkages), is translated into analogous physicochemical properties: MO245 EPS is a flexible polyelectrolyte, with scaling exponents similar to that described for HA. This similitude opens opportunities in future drug delivery, tissue engineering, and cosmetic applications.

Keywords

exopolysaccharide, hyaluronic-like, NMR spectroscopy, physicochemical properties, bacterial mats, *Vibrio sp*

1. Introduction

Polysaccharides are a promising ecological alternative to substitute materials from fossil fuel industry as they are renewable, lightweight, and not pollutant and the most abundant organic material in the world. Among the common sources of polysaccharides fungi and bacteria have the advantage to allow the production with a high structure reproducibility (Donot, Fontana, Baccou&Schorr-Galindo, 2012). Exopolysaccharides (EPSs) are secreted from microorganisms into their surrounding environment and usually help cells in surface adhesion. Under abundance of sugars EPSs are overproduced to become reserves of carbohydrate for subsequent metabolism. Some microorganisms can produce and excrete over 40 g/L of EPS in simple production conditions (Donot, Fontana, Baccou & Schorr-Galindo, 2012). This situates EPSs as important products of microbial biotechnologies and their isolation, characterization and laboratory production has been addressed thoughtfully (Nwodo, Green, & Okoh 2012). EPSs found applications in many industrial sectors, such as cosmetics and cosmeceuticals (Corinaldsi, Barone, Mercellini,

Dell'Anno & Danovaro, 2017), biosorbents (Gupta, Nayak & Agarwal, 2015), antibiofilm agents (Guezennec et al., 2012), drug delivery, and tissue engineering (Zanchetta, Lagarde & Guezennec, 2003 a; Zanchetta, Lagarde & Guezennec, 2003 b; Zykwinska, Marquis, Sinquin, Cuenot & Colliec Jouaul, 2016; Senni et al 2013).

As EPSs are ubiquitous, pioneer researches have looked into extreme habitats for EPSs with unique structure and properties. Among those extreme habitats marine ecosystems (including deep-sea, hydrothermal vents, volcanic and hydrothermal marine areas, sea ice in polar regions) are niches where extremophile bacteria prosper and can produce peculiar exopolysaccharide structures (Wang, Salem&Sani, 2019, Poli, Anzelmo & Nicolaus, 2010, Shukla, N M. Nathani & Dave, 2017; Guezennec et al., 2002; Guezennec et al., 2011). However, the full structure of most of this EPSs (beyond the monosaccharide composition) and the relation of this structure to their physicochemical and biological properties are poorly understood.

Among the several genus of bacteria that produce EPSs, *Vibrio* is one of the more widespread. It is present in marine, estuarine and freshwater systems worldwide and more than 110 species have been described (Zhang, Lin, Wang &Austin, 2018). However, the sugar compositions of only some marine *Vibrio* EPSs are known (Casillo et al, 2018) and only 2 full structures are described to date: *Vibrio diabolicus* (Rougeaux, Kervarec, Pichon & Guezennec, 1999) and *Vibrio alginolyticus* CNCM I-4994 (Drouillard et al., 2015). Both of them are composed of neutral and acidic sugars in different proportions and 1-3 or 1-4 linkages. *Vibrio alginolyticus* is the only known marine EPS with an amino acid substituent what provides interest to *Vibrio* genus in terms of potential novel structures.

A bacterium from *Vibrio* genus was isolated from bacterial Mats in the lagoon of Moorea Island (French Polynesia) and it is referred to as strain MO 245 (Guezennec et

al, 2011). Bacterial mats are laminated communities composed of phototrophic and chemotrophic prokaryotes found in lagoons in Baja California, lakes in Egypt, still waters in Spain and shallow lakes in French Polynesian atolls. They are characterized by pH values ranging from 6 to 10.5, salinity levels ranging from 5 to 42 g/L, temperatures ranging from 20 ºC during the night up to 42 ºC. Therefore, they are considered as extreme environments and produce novel molecules including polyhydroxyalkanoates and exopolysaccharides (Guezennec et al, 2001; Guezennec et al, 2011). During stationary phase of growth, the isolated MO 245 strain produces an exopolysaccharide (EPS) characterized by equal amounts of uronic acids and hexosamines (Guezennec et al, 2011). The objective of this article is to determine the structure and physicochemical properties of this polysaccharide in order to elucidate its structure-properties relationships and the potential for future cosmeceutics and biomedical applications.

2. Materials and Methods

2.1 Taxonomical studies

The phylogenetic analysis was performed by Genoscreen SAS (http://www.genoscreen.fr). A total of 1372 bp were sequenced and then a total of 1379 bp were added to an alignment of 135,717 homologous bacterial 16S rRNA primary structures by using the aligning tool of the DDBJ program package and the alignment was refined manually. Phylogenetic reconstruction was performed with the following settings as implemented in the arb software: neighbour-joining with the correction of Kimura, Maximum Parsimony and Maximum Likelihood. Different sets of filters were evaluated for the reconstruction. A consensus tree was constructed based on the topologies derived from these different analyses, included as supplementary material (Figure S1) together

with 16S rRNA sequences of the strain, designated as MO245, used in the study. This strain has been deposited in the Collection Nationale de Culture de Microorganismes (Institut Pasteur -France) as strain CNCM I-4012.

2.2 Production, isolation and purification of the polysaccharide

The polysaccharide was produced as previously described (Rougeaux, Kervarec, Pichon & Guezennec, 1999; Raguénès, Guezennec Pignet & Barbier 1997) using a 5-L bioreactor. Cells were removed from the medium by high-speed centrifugation at 20,000*g* for 2 h after around 48 h cultivation. Exopolysaccharide was precipitated from the supernatant by adding cold ethanol to a final concentration of 30% ethanol (v/v) and washed with 70–100% EtOH–water (v/v). The resulting polysaccharide was then dissolved in water and subjected to ultrafiltration using a Pellicon-2 Mini Holder equipped with a Biomax 100K filter (Millipore Corporation, Bedford, MA), washed with water, concentrated, and lyophilized. The pure EPS was then stored at room temperature.

2.3 Metal analysis by ICP-MS

Metal concentration (Na 23, Mg 24, K 39, Ca 44) were analyzed by ICP-MS (Agilent 7700x) equipped with an introduction system composed by a Micromist glass low-flow nebulizer, Scott spray chamber with Peltier (2˚C) and a quartz torch. Metal standards were measured at 0.01, 0.05, 0.1, 0.5, 1 y 10 mg/l. Ir 193 was used as internal standard.

2.4 Determination of carbohydrates composition

Neutral sugars were determined as alditol acetates as described by Nunes et al. (2012). The hydrolysis was performed with 2 M TFA at 100 ºC during 1 h for the quantification of the neutral sugars and with 6 M HCl at 100 ºC during 6 h for the quantification of the hexosamines. Uronic acids were quantified by a modification of the 3-phenylphenol colorimetric method (Nunes et al., 2012). Samples were prepared by

hydrolysis with 72% sulfuric acid for 3 h at room temperature followed by 1 h in 1 M sulfuric acid at 100 ºC. The calibration curve was performed using D-galacturonic acid. The analysis of the samples was done in quadruplicate.

The identification of the acidic monosaccharides present in the sample was performed according to Wang et al. (2017), with some modifications. 2 mg of exopolysaccharide sample were hydrolyzed with 1 mL of 2 M TFA at 120 ºC during 1 h. The sample was dried and 200 µL of 2-deoxyglucose was added as internal standard. Monosaccharides were reduced with 100 µL of sodium borohydride prepared in 3M NH_3 and heated at 30 ºC during 1 h. The reduced monosaccharides were neutralized with acetic acid and then passed through a cation exchange column (Dowex 50WX8) to remove the Na^+. The boric acid was removed by the addition of methanol (500 µL) followed by the solvent evaporation (4 times). Afterwards, the material was heated at 85 ºC during 4 h, and pyridine (200 µL) and *n*-propylamine (400 µL) were added and left to react at 55 ºC during 30 min. The acetylation was performed by adding pyridine (100 µL) and acetic anhydride (100 µL) and reacted at 95 ºC for 1.5 h. Then, distilled water and dichloromethane were added, the mixture was stirred, centrifuged, and the water was removed. The process was repeated with the addition of more distilled water and in the end the dichloromethane was evaporated to dryness. The alditol acetate derivatives formed were analyzed by gas chromatography (GC) with a 30 m column DB-225 (J&W Scientific, Folsom, CA, USA) with i.d. and film thickness of 0.25 mm and 0.15 µm, respectively, and using a flame ionization detector (Perkin Elmer, Clarus 400). The oven temperature program used was: initial temperature 200 ºC, a rise in temperature at a rate of 40 ºC/min until 220 ºC, standing for 7 min, followed by a rate of 20 ºC/min until 230 ºC and maintain at this temperature for 1 min. The injector and detector temperatures

were, respectively, 220 and 230º C. The flow rate of the carrier gas (H_2) was set at 1.7 mL/min.

2.5 Methylation analysis

Glycosidic substitution was determined by gas chromatography-quadrupole mass spectrometry (GC-qMS) of the partially methylated alditol acetates (Ciucanu & Kerek, 1984; Nunes et al., 2012). The samples were dissolved in anhydrous dimethylsulfoxide (DMSO), and then powdered NaOH was added under an argon atmosphere. The samples were methylated with CH_3I. $CHCl_3$/MeOH (1:1, v/v) was added, and the solution was dialyzed against 50% EtOH. The dialysate was evaporated to dryness and the material was remethylated using the same procedure.

One part of the dried methylated material was carboxyl-reduced to determine the glycosidic linkages of uronic acids residues (Dourado et al. 2004). Thus, 20 mg of $LiAlD_4$ and 1 mL of THF anhydrous were added to the methylated material and the mixture reacted at 65 ºC during 4 h. Two or three drops of ethanol and 2-3 drops of distilled water were added to eliminate the reagents in excess. The mixture was neutralized by adding 2 M H_3PO_4. Then, 2 mL of $CHCl_3$-MeOH (2:1 v/v) were added and the mixture was centrifuged. The supernatant (reduced polymers) were removed and the remaining white precipitate was washed 3 times more with 2 mL $CHCl_3$-MeOH (2:1 v/v). The supernatants were combined and evaporated to dryness.

The methylated and the methylated carboxyl-reduced material was hydrolyzed with 2 M TFA (1 mL) at 120 °C for 1 h, and then reduced and acetylated as previously described for neutral sugar analysis (using $NaBD_4$ instead of $NaBH_4$). The partially methylated alditol acetates (PMAA) were separated and analyzed by GC–qMS (GC-2010 Plus, Shimadzu). The GC was equipped with a DB-1 (J&W Scientific, Folsom, CA, USA)

capillary column (30 m length, 0.25 mm of internal diameter, and 0.10 µm of film thickness). The samples were injected in "split" mode with the injector temperature at 250°C. The temperature program used was as follows: an initial temperature of 80 °C; an increase of 7.5 °C/min until 140 °C, and a hold time of 5 min; an increase of 0.2 °C/min until 143.2 °C; an increase of 12 °C/min until 200 °C; an increase of 50 °C/min until 250 °C and a hold time of 5 min. The carrier gas has helium with a flow of 8.5 mL/min. The GC was connected to GCMS-QP 2010 Ultra Shimadzu mass quadrupole selective detector operating with an electron impact mode at 70 eV and scanning the range m/z 50–700 in a 1 s cycle in a full scan mode acquisition.

2.6 NMR spectroscopy

The NMR sample of MO245 polysaccharide was prepared by weighting 20 mg of the dry polysaccharide and dissolving in 0.5 mL of a solution containing D_2O (99.98%) and 0.33 mg of 3-(trimethylsilyl)-propionic acid-d_4 (TSP) that was used for internal chemical shift reference. The sample was transferred to a conventional thin-walled 5 mm NMR tube.

NMR spectra were acquired in two NMR spectrometers; one is a 750 MHz on a Varian/Agilent Inova 750 spectrometer equipped with a $^{1}H/^{13}C/^{31}P$ inverse detection probe with Pulse Field Gradients capability (PFG), and the other is an 800 MHz Bruker AVANCE-II 800 spectrometer equipped with an inverse detection $^{1}H/^{13}C/^{15}N$ CPTCI cryoprobe with PFG capability. The type of spectrometer used is indicated in each case. Proton and carbon chemical shifts were referenced to the signals of TSP which resonate at 0 ppm in both ^{1}H and ^{13}C. MestreNova software v12.0 (Mestrelab Research Inc.) was used for spectral processing and analysis.

Quantitative 1D ^{1}H NMR spectra were measured at 750 MHz and used to determine the monosaccharide composition by integration of the corresponding anomeric peaks. The spectra were measured at three temperatures of 25, 50 and 60 ºC to avoid the overlapping of some anomeric peaks with the residual HDO peak. Each spectrum was acquired with 128 scans and with the inter-scan relaxation delay (d_1) was set to 10 s to assure complete relaxation after each scan.

One dimensional ^{1}H diffusion-filtered spectrum was measured was measured at 60 ºC under conditions that completely remove the residual HDO peak thus simplifying the interpretation of the anomeric region of the polymer. The spectrum was measured with 64 scans using the Stimulated-Echo-LED pulse sequence with bipolar gradients (pulse sequence *ledbpgp2s1d*). The diffusion delay Δ was set to 100 ms, the LED period was set to 5 ms, and the duration of each PFG pulse to encode diffusion was 1 ms, with a gradient power of 47 G/cm.

Two dimensional spectra TOCSY, NOESY and H2BC were measured at 60 ºC in the 750 MHz spectrometer using standard pulse sequences from the Varian Chempack v7.0 library (pulse sequences: zTOCSY, *NOESY and h2bcetgpl3,* respectively). The TOCSY and NOESY spectra were measured with suppression of the residual HDO water peak at ~4.5 ppm by presaturation. Two TOCSY spectra were measured with DIPSI-2 spin-lock sequence and mixing times of 20 and 80 ms. The NOESY spectrum was measured with a mixing time of 100 ms.

A two dimensional pure-in-phase CLIP-COSY spectrum (Koos et al, 2016) was measured at 60 ºC in the 750 MHz spectrometer. The overall duration of the perfect echo was optimized for $^{n}J_{HH} > 2$ Hz corresponding to a duration of 50 ms. A diffusion-filter element was incorporated at the beginning of the pulse sequence for the clean removal of

the residual HDO peak. The spectrum was measured in ca. 3 h with 24 scans and 160 complex points in the indirect dimension.

Two dimensional spectra COSY, TOCSY, NOESY and H2BC were measured at 60 ºC in the 750 MHz spectrometer using standard pulse sequences from the Chempack v7.0 library that was provided by the manufacturer of the spectrometer (pulse sequences cosygpppqf, *zTOCSY, NOESY and h2bcetgpl3,* respectively). COSY, TOCSY and NOESY spectra were measured with suppression of the residual HDO water peak at ~4.5 ppm by presaturation. Two TOCSY spectra were measured with mixing times of 20 and 80 ms. The NOESY spectrum was measured with mixing time of 100 ms.

A 2D CLIP-HSQC spectrum (Enthardt, Freudenberger, Furrer, Kessler, Luv, 2008) was measured at 60 ºC in the 750 MHz spectrometer. This experiment provides a ^{1}H-^{13}C coupled spectrum in the proton F2 dimension from which the one-bond carbon proton scalar coupling ($^{1}J_{CH}$) can be determined. For sugars adopting a chair conformation, the value of the $^{1}J_{CH}$ coupling at the anomeric position determines the axial or equatorial configuration of the anomeric proton. A value of ~170 Hz for $^{1}J_{C1H1}$ indicates an equatorial proton at C-1, e.g. α-D-glucose, while $^{1}J_{C1H1}$ of ~160 indicates an axial proton, e.g. β-D-glucose (Bubb, 2003). The spectrum was measured with 128 scans and 70 complex points in t_1. To save measurement time a reduced ^{13}C spectral window in the region of interest (67-120 ppm) was selected.

Two-dimensional spectra HSQC and HMBC were measured at 60 ºC in the 800 MHz spectrometer using standard pulse sequences from the Bruker library (pulse sequences *hsqcetgpsi* and *hmbcgplpndqf*, respectively). The HSQC spectrum was measured with 8 scans and 256 complex points in the t_1 dimension. The relaxation delay d_1 was 1 s. The HMBC spectrum was measured in the magnitude mode with 496 scans

and 512 points in t_1. The delay for the evolution of long range $^{n}J_{CH}$ coupling in the HMBC sequence was optimized for a nominal value of 7 Hz. The relaxation delay d_1 was 1.1 s.

A DOSY spectrum was measured at 60 ºC in the 750 MHz spectrometer with the sequence single stimulated echo BPP-LED-STE experiment. The gradient pulses that encode diffusion were varied linearly between 2.66 and 53.3 G cm^{-1} along 32 points in the diffusion dimension. The duration of each pair of bipolar gradients δ was 8 ms and the diffusion time Δ was 500 ms. The spectrum was acquired with a relaxation delay d_1 of 2 s, an acquisition time of 2.75 s and 64 scans per each point in the diffusion dimension. The total measurement time was ~2 h 30 min. After Fourier transformation in the ^{1}H dimension, several peaks were selected for the analysis of the self-diffusion coefficient. In each case the peak intensity along the diffusion dimension was fitted to the mono-exponential Stejskal-Tanner equation using software Origin 8.0 (*Originlab inc.*) to determine the self-diffusion coefficient (D).

2.7 Gel Permeation Chromatography (GPC)

GPC with RALS and Viscometer: measurements were performed on a Malvern Viscotek TDA 305 with refractometer, right angle light scattering and viscometer detectors. Samples were measured with a Suprema Precolumn (5 μm, 8×50 mm), Suprema 30 Å (5 μm, 8×300 mm), Suprema 1000 Å (5 μm, 8×300 mm) and PLaquagel-OH-Mixed (8 μm, 7.5×300 mm). The system was kept at 30 ºC and 0.1 M NaN_3 in 0.01 M NaH_2PO_4, at pH 6.6, was used as eluent at a rate of 1 mL/min. Pullulan with 47 kDa and polydispersity index (PDI) 1.07 (PSS standard services) was used to obtain a multidetector calibration. The refractive index increment (dn/dc) was determined on-line from the RI detector response assuming that sample concentration is accurate, as recommended by Malvern, and determined as 0.124±0.02.

GPC with MALS: measurements were performed on a LC system consisting of Agilent-SECcurity-Pump and an Agilent-SECcurity Autosampler connected to a refractive index (PSS-SECcurity DRI) and multi angle static light scattering (PSS SLD 7100 MALLS) detectors. Samples separation was achieved using 4 columns (PSS, Mainz, Germany): Suprema precolumn (10µm, 8x50mm), 3x Suprema ultrahigh (10µm, 8x300mm). Column and detectors were kept at 35 ºC. Samples were eluted with PBS buffer (0.01 M phosphate buffer, 0.0027 M potassium chloride and 0.137 M sodium chloride, pH 7.4) pumped at a constant rate of 0.5 mL/min. The light scattering detector was calibrated with a pullulan standard (PSS, Mainz, Germany) of Mw 100 kDa and polydispersity index (PDI) 1.09. The dn/dc was calculated on-line from the RI detector response assuming that the concentration of the polymer solution is accurate and determined as 0.123.

2.8 Dynamic light scattering

DLS was performed at an angle of 173° and room temperature. The average hydrodynamic diameter (Rh) and polydispersity index (PDI) were determined by fitting the correlation function with the cumulant method. The EPS was dissolved in PBS buffer (0.01 M phosphate buffer, 0.0027 M potassium chloride and 0.137 M sodium chloride, pH 7.4) at 0.125, 0.25, 0.5 1.0, 2, 5, 10 g/L. The measurements at each concentration were repeated 5 times. The mean Rh and PDIs for each concentration are included in Table S6. For concentrations lower than 0.25, count rate was too low for an accurate measurement. For concentration higher than 2 g/L, an additional diffusion mode appears in the correlogram and PDI bursts to 1 hindering the determination of Rh. For intermediate concentrations (0.25, 0.5 g/L) Rh were similar and PDI. The Rh included in Table 4 was

determined at 0.25 g/L since at this concentration we have enough scattering and a the lowest PDI (0.38).

2.9 Rheology

The studies were performed with Malvern Kinexus Rotational Rheometer, UK. Shear viscosity was measured with a stainless steel cone-plate geometry at 25.0 ± 0.1 °C with a 4°/40 mm geometry between 1 and 1000 s^{-1}. Oscilatory test was performed with a stainless steel parallel plate geometry with 20 mm of diameter. The linear viscoelastic region was first determined by an amplitude sweep stress controlled experiment with a frequency of 1Hz. Then frequency sweep strain controlled experiments were performed between 10 and 0.1 Hz at a shear strain inside the viscoelastic region (5%). The EPS was dissolved in PBS buffer (0.01 M phosphate buffer, 0.0027 M potassium chloride and 0.137 M sodium chloride, pH 7.4) at 1, 2, 2.5, 1.87, 2.5, 3, 3.75, 5, 6, 7.5, 10, 15, 20, 25, 30, 40 g/L.

2.10 Complexation with $CuCl_2$ and $CaCl_2$

1 mL of 20 g/L, 10 or 5 g/L solutions of MO245 (in PBS buffer or water) where added over 1 mL of a 10g/L solution of $CuCl_2$ or $CaCl_2$ (in PBS buffer or water) and manually mixed. The formation of the gel was detected by inversion test after 1 min and confirmed after 1, 2 and up to 24 h. Gels were immediately formed only for the 20 g/L MO245 added to $CuCl_2$ solution independently of the solvent (water or PBS). Concentrations below 20 g/L and addition to $CaCl_2$ revealed no gel formation in the inversion test.

3. Results

3.1 Taxonomy, isolation and purification

The sequence of the 16S rRNA encoding gene of strain MO245 was determined (1372 bp) and deposited in the DDBJ sequence database. Phylogenetic analyses using the NCBI´s Basic Local Alignment Search Tool (BLAST) program showed that strain MO245 belonged to the gamma subdivision of the phylum Proteobacteria, which is part of the *Vibrio* genus and closely related to *Vibrio alginolyticus.*

The polysaccharide was produced following previous well-established conditions for EPS production in a 5-L bioreactor (Rougeaux, Kervarec, Pichon & Guezennec, 1999; Raguénès, Guezennec Pignet & Barbier 1997), cells were separated by centrifugation and the EPS precipitated with a hydro-alcoholic solution and purified again by ultrafiltration (100 kDa membrane) leading to a yield near 3 g/L of polysaccharide without optimization studies. A low metal (Na, Mg, K, and Ca) content was determined by ICP-MS. Na accounted for 2.125%±0.003 of mass of weight EPS, 0.028%±0.006 for Mg, 0.083%±0.008 for K, and 0.422±0.010 % for Ca.

3.2 Exopolysaccharide structural analysis

The monosaccharide composition of this polysaccharide was already reported together with the properties of several EPS from bacterial mats found in French Polynesia (Guezennec et al., 2011). The herein performed monosaccharide composition analysis confirmed the presence of equal amount of uronic acids (determined as glucuronic acid) and hexosamines, being the last composed by the same proportion of GalN and GlcN (Table 1). When the hydrolysis was performed with 2 M TFA or 1 M H_2SO_4 (conventional hydrolysis conditions for neutral polysaccharides) the percentage of GalN and GlcN was much smaller and most of the sample seemed to be composed of GlcA. Only a hydrolysis with 6 M HCl during 6 h allowed to determine the accurate content of

the amino sugars. This difficulty in hydrolyzing this polysaccharide is related with the presence of aldobiouronic disaccharides (Ferreira et al., 2011), demonstrating the presence of linkages between the GlcA and both GalN and GlcN. The sugar composition showed also the presence in minor quantities of other neutral sugars (< 3%), galactose and rhamnose (again in agreement with previous data) and glucose that was not observed previously. The main structure, according to the amount determined of each sugar, appears to be composed of a tetrasaccharide repeating unit with two GlcA units and two hexosamines (possibly one acetylated GalN and one acetylated GlcN).

The methylation analysis revealed that GalN is (1→4)-linked (52 mol%) and GlcN is (1→3)-linked (42 mol%), with small amount of (1→6)-linked hexosamine and (1→3)-linked GalN. It was only observed trace amounts in the samples of terminally linked GalN, indicating that it is linear polysaccharide with high molecular weight. The methylation was also performed with and without carboxyl reduction and, although the results are non-quantitative due to the non-stochiometric carboxyl reduction of GlcA to Glc, it was possible to detect terminally linked GlcA and (1→4)-linked GlcA. In this way, the EPS of MO245 is linear, composed of (1→4)-GalN, (1→3)-GlcN, and (1→4)-GlcA. In order to elucidate the complete structure of the EPS (presence of acetylated hexosamines, anomeric configuration of the sugars, sugar arrangement) NMR spectroscopy experiments were performed.

The ^{1}H NMR shows the typical broad signals and a high overlap between 4 and 3.2 ppm, as expected for a complex polysaccharide with high molecular weight. Four signals are distinguished in the anomeric region (labeled in Figure 1) at 5.40, 4.66, 4.59 and 4.52 ppm). Other two minor anomeric signals with ca. 5% of intensity compared to the main signals appear at 5.23 and 5.18 ppm. The two strong signals at 2.05-2.15 ppm are consistent with the presence of two N-acetylated sugars in the structure and a weak

methyl signal at 1.27 ppm indicates traces of fucose or rhamnose (rhamnose according to the sugar composition). The ^{1}H spectra agrees well with the data obtained in the monosaccharide composition.

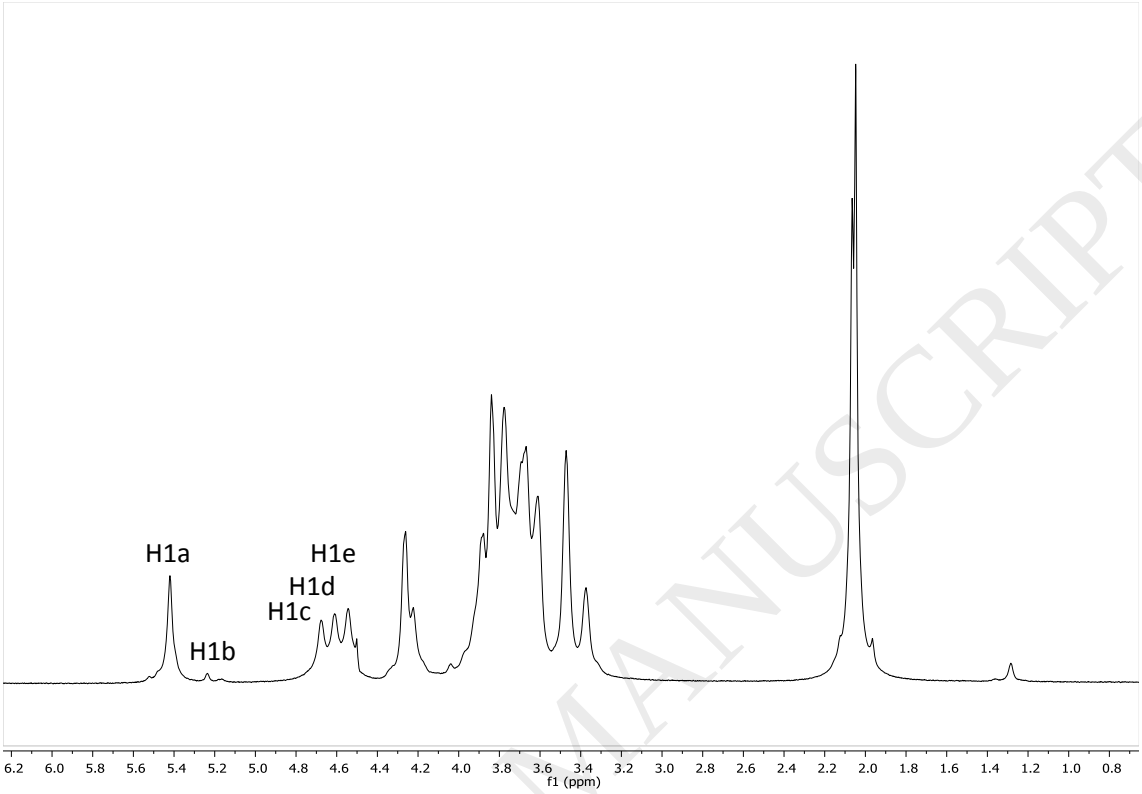

Figure 1. ^{1}H NMR Diffusion filtered spectrum (D_2O, 60ºC, Δ=100ms, δ=1ms, 750 MHz) of the EPS from MO245. The five most intense anomeric peaks are labelled.

The assignment of the ^{1}H and ^{13}C NMR resonances of MO245 in each residue (Table 2) was obtained by a combination of the following 2D homo- and heteronuclear 2D spectra: CLIP-COSY, TOCSY, NOESY, HSQC, H2BC, HMBC and CLIP-HSQC (Figures S2-S10). A more detailed description of the signal assignment is included in the supplementary material.

The type of glycosidic linkage connecting the pairs of monosaccharide units in the structure of MO245 was deduced from the observation of HMBC inter-residual

correlations (H1c-C4a, H4a-C1c, H1d-C4e, H1e-C4c and H4c-C1e, and H3d-C1a, Fig. S5b and Table S1) and agrees with the NOE cross peaks (detailed in the supplementary material). According to these peaks we deduce the following repeating unit for the EPS chain of MO245:

→4)-β-D-Glc*p*A-(1→4)-α-D-Gal*p*NAc-(1→3)-β-D-Glc*p*NAc-(1→4)-β-D-Glc*p*A-(1→

c **a** **d** **e**

Figure 2: Structure of EPS MO245 and the letter code used for the NMR assignment

There is in agreement with the $^{1}H/^{13}C$ experimental chemical shifts of MO245 of Table 2 and those empirically predicted by the Bacterial Carbohydrate Structure Database (http://csdb.glycoscience.ru/bacterial/) for the structure of MO245 proposed in Figure 2 (Tables S3). The structure deduced for MO245 is identical to that proposed *Vibrio diabolicus* strain named HE800 (Rougeaux, Kervarec, Pichon & Guezennec, 1999). The ^{1}H NMR spectra of these polysaccharides is almost a fingerprint copy of the one described for HE800 (Figure S10) and the reported experimental ^{1}H and ^{13}C are essentially identical to those obtained for MO245 (see Table S4 and S5).

For MO245 there is also the presence of a minor proportion (ca 5%) of other sugars (glucose galactose, and rhamnose) that are not described for HE800. These additional sugars also appear in the TOCSY/HSQC spectra, although in much lower intensity. For instance, the anomeric proton or residue b, H1b (5.21 ppm) correlates to 4.3 and 3.45 in the TOCSY and 98.8 ppm in the HSQC. A second example is the peak of the methyl group the rhamnose at $^{1}H/^{13}C$ 1.27/19.4 ppm that appears in the HSQC (Fig. S4). A DOSY spectrum was measured and the diffusion coefficient corresponding to the glucose, galactose and rhamnose are very similar to those of the MO245 (Figure S11) and are, at least, one order of magnitude lower that the values expected for mono or oligosaccharides (Viel, Capitani, D., Mannina & Segre, 2003). In addition, a small amount of the already

purified sample of MO245 was further repeatedly ultrafiltered with a 100 kDa cut off regenerated cellulose membrane using first NaCl 0.2 M (to remove impurities linked by any electrostatic interaction) and then water. The minor sugar components appear, in the same proportion as before, in the ^{1}H spectrum after ultrafiltration (Figure S12b) and present also similar proportion is MO245 obtained in different fermentations (Figure 1 vs Figure S12a). Altogether, this points to the glucose, galactose and rhamnose residues covalently-linked at specific points in the polysaccharide chain.

The similarity found between MO245 and HE800 structures raises an interesting query about the occurrence of the same *Vibrio* sp both nearby hydrothermal vents associated with extreme conditions and microbial mats present in atolls in French Polynesia and suggests that further taxonomical studies are required. Moreover, not only further taxonomical but also further structural studies are necessary to picture common features of the EPS from *Vibrio* species since the herein presented is only the third full structure described for a EPS from *Vibrio* from the more than 100 described taxonomically (Casillo et al., 2018). The other *Vibrio* EPS with known structure is *Vibrio alginolyticus* CNCM I-4994 (Drouillard et al., 2015): [3)-α-D-GalA-(1→4)-α-D-GalA-(1→3)-α-D-GalA-(1→3)-β-D-GlcNAc-(1→] where also a linked aminoacid is present in some repeating units. This is relatively similar structure to MO245 but with a much higher proportion of uronic acids. For other structures of *Vibrio* EPSs only the monosaccharide composition is known. Those EPSs usually contain also uronic acid and N acetylated sugars but also other neutral sugars in lower proprortion as observed for MO245 (Casillo et al, 2018).

There is also a similarity between the structure of MO245 and HE800 to that of hyaluronic acid. This proposed resemblance is based in an equal ratio of GlcA to N-acetylated sugars and in the same type of glyosidic linkages present in the repeating unit

(alternated 1→3 and 1→4 linkages). These similitudes (and differences) open an interesting question on the relationship between the structure and the physicochemical and biological properties of MO245 EPS versus hyaluronic acid. Therefore, the results from the conformational and rheological characterization of MO245 EPS will be compared with the literature data available for HA, along the rest of the manuscript.

3.3 Molecular weight and conformation

The molecular weight of MO245 EPS was initially determined in a GPC system equipped with a triple detector (RALS, LS detected at 90º), refractometer (RI), and viscometer. This configuration provides the absolute molecular weight and allows the simultaneous determination of the intrinsic viscosity of the EPS. The GPC chromatogram of MO245 is shown in Figure 3 and the obtained values in Table 3.

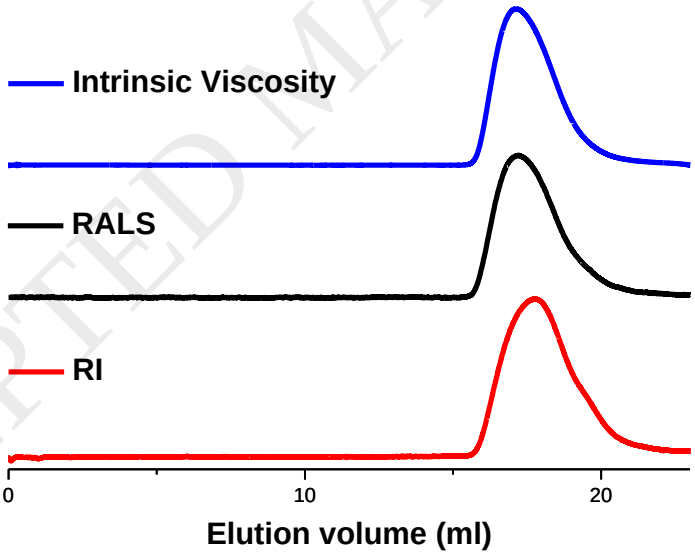

Figure 3. GPC eluograms of CS from MO245 EPS in 0.1 M NaNO3, 0.01 M NaH2PO4, pH 6.7. The refractive index, intrinsic viscosity and right angle light scattering detector signals are signed in colors.

A polymeric peak is observed at 17.9 mL in the refractive index (RI) with only slight difference in retention time and in the viscosity in light scattering detectors. Although the configuration of the equipment with the laser at 90 ºC gives the best signal to noise ratio, the angle dependence of the LS signal limits the M_w range. The value obtained for the weight average molecular weight M_w of the EPS, 536 kDa, is on close to such limit (Table 3). Therefore, we have used also an equipment with a LS detector at 7 angles. In this equipment the M_w measured is similar, 513 kDa, showing the RALS data is not biased by due to angle dependence (Table 3 and Figure S13). The Mw found for MO245 is lower than for the biopolymer produced by strain HE 800 ranging from 900 to 1500 kDa (Rigouin et al 2012; Zykwinska et al 2016).

The on-line coupling of the intrinsic viscosity in the first GPC measurement allows to obtain the slope of the intrinsic viscosity versus the log of molecular weight, α (Figure S14). The on-line coupling of the SLS at several angles in the second GPC measurement allows to obtain the slope of R_G versus the log of molecular weight *v* (Figure S13). We found $[\eta] \sim M_w^{0.81}$ and $R_G \sim M_w^{0.70}$ (Table 3). Those exponents can be related to polymer conformation and are near to the values theoretically predicted and experimentally found for flexible polyelectrolytes in a good solvent (Dobrynin, Colby, Rubinstein, 1995), and similar to the values described for HA (Cowman & Matsuoka, 2005, included in Table 3 for comparison purposes).

The static light scattering data have been complemented with the measurements of the dynamic light scattering measured at 7 concentrations, between 0.125 and 10 g/L. The correlation functions showed one size distribution that decays simultaneously up to 1 g/L. This decay can be related to the hydrodynamic radius of the EPS in solution that results in a R_h of 42 nm using the cumulant algorithm (Table 3). This hydrodynamic radius measured by DLS is in good agreement with the hydrodynamic radius determined with

the on-line viscosity detector by GPC (37 nm). Over 1 g/L (at 2, 5 and 10 g/L) a second decay appears (Figure 4).

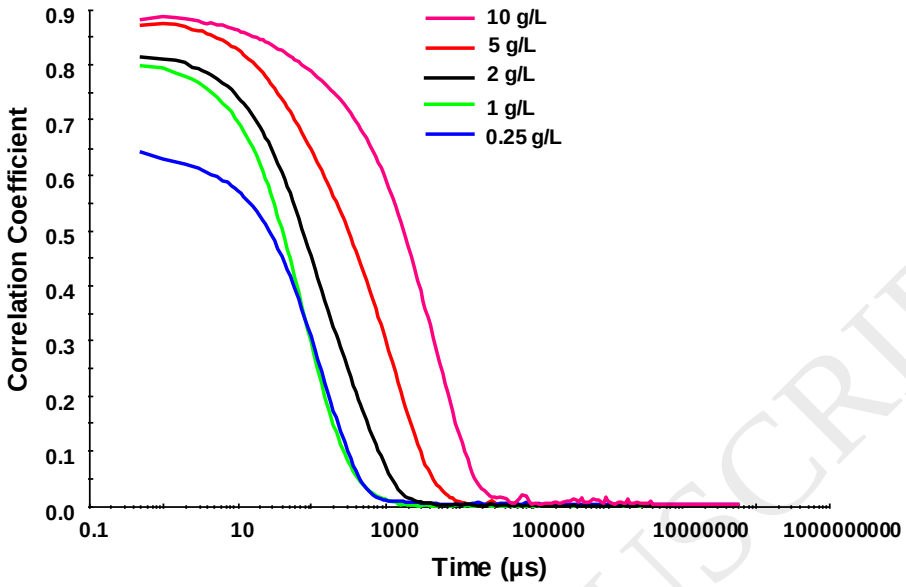

Figure 4. Dynamic light scattering correlograms of MO245 in PBS at 5 representative concentrations.

This second decay (or slow mode) can be related to the formation of aggregates or to the diffusion of polymer domains over the overlap concentration and is typically found in the DLS of polyelectrolytes, including HA (Esquenet & Buhler, 2002). This means that MO245 has a polyelectrolyte behavior similar to HA and also that the semi dilute regime (regime over the overlap concentration) in MO245 starts over 1 g/L. Moreover, the R_g/R_h ratio is lower than in the case of HA: ca 1.8 in HA, and 1.33 here (see Rg and R_h in Table 3), pointing to a less extended conformation of MO245 versus HA. This last observation is reinforced by the lower [η] found for comparable Mw HA (see experimental values and literature data in Table 3).

3.4 Rheological behaviour of MO245 at physiological conditions

The structural similitude of the EPS MO245 to hyaluronic acid opens, in our opinion, a variety of potential applications of MO245 in cosmetics and regenerative medicine. In fact, marine EPSs from HE800 with very similar structure to MO245 has been proposed alternative to HA in such applications (Senni &Colliec-Jouault, 2011). The importance of HA structural role in the ECM of mammalian has led to rheological analyses of HA solutions already in the 50s of the 20th century when its structure was only recently elucidated (Balazs &. Laurent, 1951; Selyanin, Boykov, Khabarov, & Polyak, 2015). This and numerous subsequent studies (Morris, Rees, & Welsh, 1980; Yanaki, & Yamaguchi, 1990; Fouissac, Milas, & Rinaudo, 1993; Berriaud, Milas & Rinaudo, 1994; Fouissac, Milas, Rinaudo, & Borsali, 1992; Milas. Roure& Berry, 1996; Fukada, Suzuki, & Seimiya, 1999, Mo, Takaya, Nishinari, Kubota, K., & Okamoto, 1999, Takahashi, Kubota, Kawada & Okamoto, 1999) have revealed the importance of the ionic strength in the viscosity of HA, as expected for a polyelectrolyte. Therefore, an analysis of MO245 viscosity at physiological conditions (pH, and ionic strength) was performed and compared with a study of HA in the exactly same solvent (Krause, Bellomo, & Colby, 2001). With this purpose, it was determined the viscosity of MO245 solutions in phosphate buffered saline at 14 concentrations between 1 to 40 g/L with increasing shear rate (representative concentrations are shown in Figure 3).

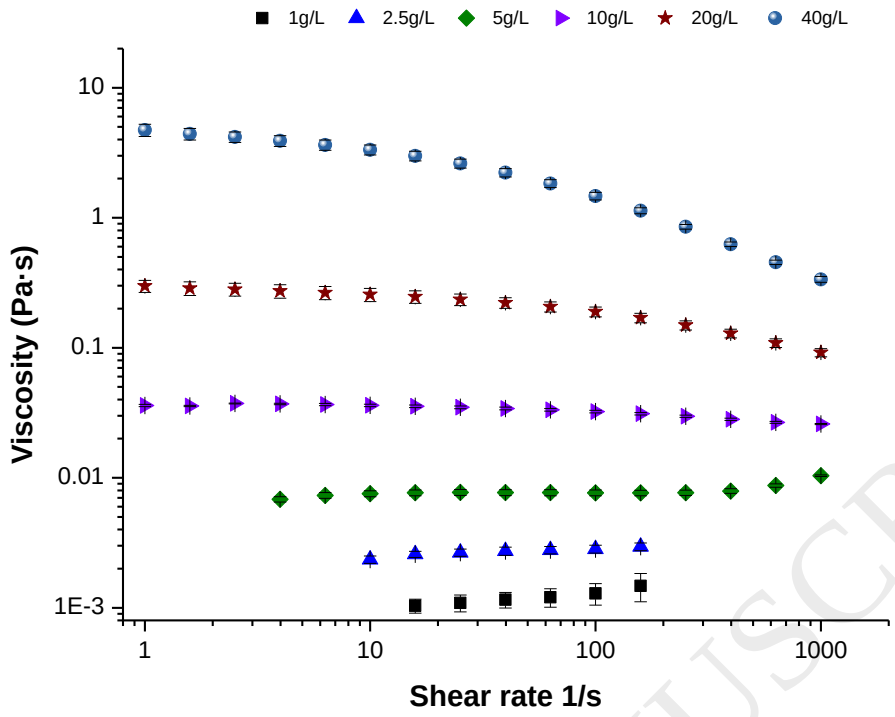

Figure 5. Shear Viscosity of MO245 solution in PBS of MO245 in PBS at 25 °C.

MO245 solutions showed, as most polysaccharides, a Newtonian behaviour at low concentrations and a pseudo plastic behaviour (shear tinning over a critical shear rate) for high concentrations, what happens in MO245 over 10 g/L (red stars and blue circles). At these concentrations, 20 and 40 g/L, oscillatory mechanical test (frequency sweep strain controlled oscillatory experiments) showed the viscoelastic character of MO245 solutions (Figure 6). MO245 dissolved in PBS is not a gel since G´´ is higher than G´ at low frequencies and a crossover of the moduli happens around 10 Hz. A step increase of the elasticity occurs as the frequency grows as observed from the relative increase of G´ to G´´, a viscoelastic behaviour that is characteristic of numerous high molecular weight polymers, including HA (Gibbs, Merrill & Smith K1968; Takaya, Nishinari, Kubota, K., & Okamoto, 1999).

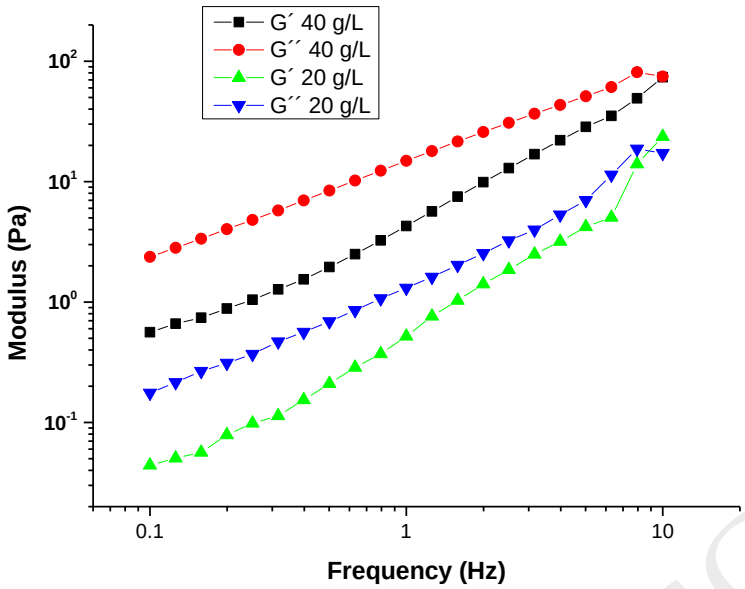

Figure 6. Elastic (G') and viscous (G") moduli of a solution of MO245 at 20 and 40 g/L (PBS buffer) determined in a frequency sweep strain controlled experiment performed between 10 and 0.1 Hz at a shear strain inside the viscoelastic region (5%).

To gain additional information on MO245 solution properties the specific viscosity was is represented *vs* the concentration, a common method to determine the scaling behaviour (related to the polymer conformation and solvent quality) and the change from dilute to semidilute and, semidilute unentangled to semidilute entangled, regimes (Figure 6). The zero-shear rate viscosity, η_0 was extrapolated from the viscosity shear rates plots. From the value of η_0 the specific viscosity was determined as $\eta_{sp} = (\eta_0 - \eta_s)/\eta_s$.

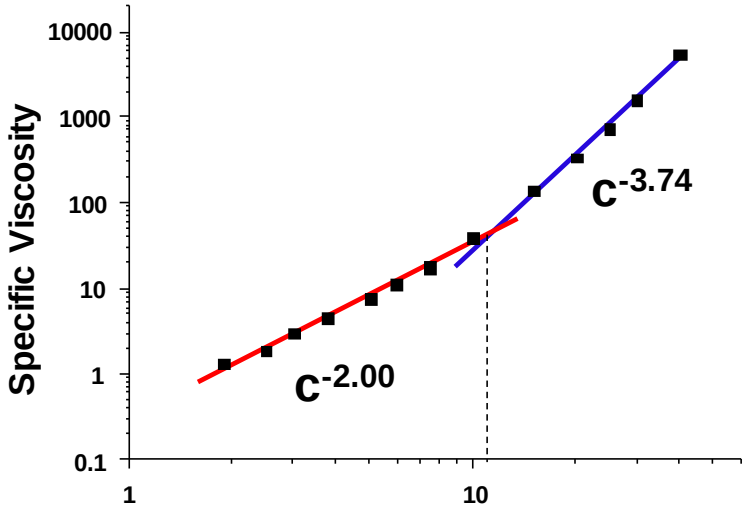

Figure 7. Concentration dependence of the specific viscosity of MO245 in PBS at 25 °C.

An accurate determination of the viscosities at concentration below 1g/L was difficult and hampered the determination of the scaling behaviour in the dilute regime. Nevertheless, the overlap concentration can be estimated as the point where the specific viscosity is twice the solvent viscosity, which happens at 2.5 g/L. Over this concentration the plot of η_{sp} vs c shows the transitions from the unentangled and entangled regime (Figure 7). The slope of these logarithmic plots gave scaling behaviour of $\eta_{sp} \sim c^{-2.00\pm0.05}$ and $\eta_{sp} \sim c^{-3.74\pm0.16}$ respectively and the intercept of both lines an entanglement concentration C_e of 10.9 g/L.

The scaling behaviour agrees again with the predictions for flexible polyelectrolytes in the high salt limit and are similar to that observed for HA at physiological conditions with a slightly lower value of the entanglement regime (4.1 found for HA, Krause, Bellomo, & Colby, 2001). The herein found exponent agrees w with the value predicted by Dobrynin ($\eta_{sp} \sim c^{15/4}$, Dobrynin, Colby, & Rubinstein, 1995). The comparison of the η, C^*, C_e of HA, vs MO245 is difficult since meaningful comparison accounts only for very similar M_w, solvent and concentrations. However,

MO245 appears to be less viscous than HA, 50 mPa for HA with 860 kDA in 0.1 M NaCl at 5g/L (Berriaud, Milas & Rinaudo. 1994) versus the herein found 5 mPa for MO245, and have a higher C*: 0.8 g/L found for 610 kDa HA in 0.1 M NaCl (Esquenet & Buhler, 2002) versus the herein found ~2.5 g/L. This observation reinforces the previous indications (Rg/Rh ratio and lower $[\eta]$) of a less extended conformation in MO245 than in HA.

3.5 Gel formation with divalent cations: Cu versus Ca.

To further compare the behaviour of MO245 versus HE800 and HA the complexation of MO245 to divalent cations, calcium and copper, was studied. The immediate gelation by addition of Cu^{2+} salts (but not to Ca^{2+}) has been recently described for HE800 solutions, but does not occur in HA (Zykwinska, Marquis, Sinquin, Cuenot, & Colliec-Jouault, 2016).

In the case of MO245, the mixture of equal volumes of (10 g/L) solutions (both in PBS buffer or water) with $CuCl_2$ and $CaCl_2$ solutions lead to instantaneous formation of gel with Cu, but not with Ca (images of the inversion test in Figure S16). Interestingly, and relating to the rheology, the gelation occurs when the solution of MO245 is over the entanglement concentration (and therefore chains are close enough to form the gel bridges) but not for concentrations lower than 10 g/L (C_e determined was 10.9 g/L).

The reason why MO245 and HE800 form gels but HA doesn't is explained by the egg-box model described for alginate gel formation with divalent cations. In the egg-box model intermolecular bridges between two polysaccharide chains are formed between 4 uronic acid units (two in each chain) complexed to one divalent metal cation (Li, Fang, Vreeker & Appelqvist ,2007). This strong intermolecular complexation is only possible if at least 2 consecutive uronic acids are present in the structure, as it happens in

alginate (with long uronic acid sequences), HE800 and MO245 (with only two consecutive uronic acids), but not in HA that consequently does not gel with divalent cations. The reason why MO245 form gels with Cu but not with Ca (as it happens in alginate) is the reported stronger affinity for Cu compared to Ca of uronic acid containing polysaccharides (alginate or pectin, Smidsrød & Gudmund, 1990, Ouwerx, Velings, Mestdagh, & Axelos, 1998). In alginate or pectin the long uronic acid sequences allow the formation of strong intermolecular bridges for the less strongly chelating Ca while in the case of MO245, and HE800 (only two consecutive uronic acids) the gelation is restricted to the stronger chelating Cu. The observed complexing ability in MO245 can be useful for future applications not only for the formation of macroscopic gels but also for micro and nano-fabrication (Zykwinska, Marquis, Sinquin, Cuenot, & Colliec-Jouault, 2016).

4. Conclusions

The structure of an MO245 exopolysaccharide from *Vibrio sp*. isolated from bacterial mats in Moorea Island consists of a linear tetrasaccharide repeating unit with the following repeating unit:

[-4)-β-D-GlcpA-(1→4)-α–D-GalpNAc-(1→3)-α–D-GlcpNAc-(1→4)-β–D-GlcpA(1→]

The structure is identical to that found for a bacterium from deep see hydrothermal vents *Vibrio diabolicus* (EPS HE800) with exception of a small proportion (ca. 5% in NMR and 3 % in GC) of glucose, galactose, and rhamnose residues that seem to be covalently-linked to the main backbone.

The average molecular weight was determined to be 513±4 (PDI 1.42±0.01) kDa. The viscosity vs M_w, Rg vs Mw from the GPC study and the rheological analysis reveals MO245 as a weak polyelectrolyte with similar conformational properties than HA and a

slightly less extended chain in solution. Over the entanglement concentration gelation of MO245 with copper divalent anions occurs. The proposed structural similitude of MO245 to HA (in terms of proportion of uronic to N-acetylated sugars and glyosidic linkages) leads to similar physicochemical properties (observed by light scattering and rheology) of MO245 EPS and HA. In our opinion, this similitude confers a great interest to the herein presented polysaccharide for future applications in pharmaceutical, cosmeceutical and tissue engineering applications.

Acknowledgements

We thank the NMR technical facilities of RIAIDT, CACTUS at the University of Santiago de Compostela and in the "Manuel Rico" NMR laboratory (LMR) of the Spanish National Research Council (CSIC) were the 750 MHz and 800 MHz NMR spectra were carried out respectively. FCT/MEC for the financial support to CICECO (FCT UID /CTM /50011/2013; POCI-01-0145-FEDER-007679) and QOPNA research Unit (FCT UID/QUI/00062/2013), through national founds and co-financed by the FEDER, within the PT2020 Partnership Agreement. RNC (IF/00373/2014), CN (SFRH/BPD/100627/2014), and ASF (SFRH/BD/102471/2014) thank the FCT foundation for funding. We thank Dr Stephane Cerantola (UBO Brest) for providing the ^{1}H NMR spectrum of HE800 for comparison purposes.

References

Balazs, E. A., & Laurent, T. C. (1951). Viscosity function of hyaluronic acid as a polyelectrolyte. *Journal of Polymer Science*, 6(5), 665-667.

Berriaud, N, Milas & M, Rinaudo, M (1994) Rheological study on mixtures of different molecular weight hyaluronates. *International Journal of Biological Macromolecules.* 16(3), 137-42.

Bubb, William A. (2009). NMR Spectroscopy in the Study of Carbohydrates: Characterizing the Structural Complexity. *Concepts in Magnetic Resonance Part A*, 19A, 1–19.

Casillo, A.; Lanzetta, R.; Parrilli, M.; Corsaro, M., (2018). Exopolysaccharides from Marine and Marine Extremophilic Bacteria: Structures, Properties, Ecological Roles and Applications. *Marine Drugs*, 16(2), 69-103.

Ciucanu, I., & Kerek, F. (1984). A simple and rapid method for the permethylation of carbohydrates. *Carbohydrate Res*,131(2), 209–217.

Corinaldesi, C., Barone, G., Marcellini, F., Dell'Anno, A., & Danovaro, R. (2017). Marine Microbial-Derived Molecules and Their Potential Use in Cosmeceutical and Cosmetic Products. *Marine Drugs*, 15(4), 118.

Cowman, M. K., & Matsuoka, S. (2005). Experimental approaches to hyaluronan structure. *Carbohydrate Reearch.*, 340(5), 791-809.

Dobrynin, A. V., Colby, R. H., & Rubinstein, M. (1995). Scaling Theory of Polyelectrolyte Solutions. *Macromolecules*, 28(6), 1859-1871.

Donot, F.; Fontana, A.; Baccou, J. C.; Schorr-Galindo, S., (2012). Microbial exopolysaccharides: Main examples of synthesis, excretion, genetics and extraction. *Carbohydrate Polymers*, 87 (2), 951-962.

Dourado, F.; Madureira, P.; Carvalho, V.; Coelho, R.; Coimbra, M. A.; Vilanova, M.; Mota, M.; Gama, F. M. (2004). Purification, structure and immunobiological activity of an arabinan-rich pectic polysaccharide from the cell walls of *Prunus dulcis* seeds. *Carbohydrate Research*, 339(15), 2555-2566.

Drouillard, S.; Jeacomine, I.; Buon, L.; Boisset, C.; Courtois, A.; Thollas, B.; Morvan, P.-Y.; Vallée, R.; Helbert, W., Structure of an Amino Acid-Decorated Exopolysaccharide Secreted by a *Vibrio alginolyticus* Strain. *Marine Drugs* 2015, 13(11), 6723-6739.

A. Enthart, J.C. Freudenberger, J. Furrer, H. Kessler & B. Luy, (2008**).** The CLIP/CLAP-HSQC: Pure absorptive spectra for the measurement of one-bond couplings, *Jounal of Magnetic. Resononance* 192 (2), 314-322.

Esquenet, C. & Buhler, E. (2002). Aggregation Behavior in Semidilute Rigid and Semirigid Polysaccharide Solutions. *Macromolecules*, 35(9), 3708-3716.

Fouissac, E., Milas, M., Rinaudo, M., & Borsali, R. (1992). Influence of the ionic strength on the dimensions of sodium hyaluronate. *Macromolecules*, 25(21), 5613-5617.

Ferreira, J. A.; Domingues, M. R. M.; Reis, A.; Figueiredo, C.; Monteiro, M. A.; Coimbra, M. A., Aldobiouronic acid domains in *Helicobacter pylori*. Aldobiouronic acid domains in Helicobacter pylori. *Carbohydrate Research* 346, 638–643 (2011).

Fouissac, E., Milas, M., & Rinaudo, M. (1993). Shear-rate, concentration, molecular weight, and temperature viscosity dependences of hyaluronate, a wormlike polyelectrolyte. *Macromolecules*, 26(25), 6945-6951.

Fukada, K., Suzuki, E., & Seimiya, T. (1999). Rheological Properties of Sodium Hyaluronate in Decyltrimethylammonium Bromide Aqueous Solutions1. *Langmuir*, 15(12), 4217-4221.

Gibbs D.A, Merrill E.W & Smith K.A. (1968). Rheology of hyaluronic acid. *Biopolymers*. 1968, 6(6), 777–91.

Guezennec J., Moppert X., Raguenes G., Richert L., Costa B. & Simon Colin C. (2011). Microbial mats in French Polynesia and their biotechnological applications. *Process Biochemistry*, 46 (1), 16-22.

Gupta, V.K, Nayak. A. & Agarwal S. (2015). Bioadsorbents for remediation of heavymetals: Current status and their future prospects. *Environmental Engineering Research* 20(1), 1-18

Guezennec J (2002). Deep-sea hydrothermal vents: A new source of innovative bacterial exopolysaccharides of biotechnological interest*? Journal of Industrial Microbiology & Biotechnology* 29: 204-208

Guezennec, J., Herry, J. M., Kouzayha, A., Bachere, E., Mittelman, M. W., & Bellon Fontaine, M. N. (2012). Exopolysaccharides from unusual marine environments inhibit early stages of biofouling. *International Biodeterioration & Biodegradation*, 66(1), 1-7.

Li, L., Fang, Y., Vreeker R., and Appelqvist, I. (2007). Reexamining the Egg-Box Model in Calcium−Alginate Gels with X-ray Diffraction, *Biomacromolecules*, 8 (2), 464–468

Krause, W. E., Bellomo, E. G., & Colby, R. H. (2001). Rheology of Sodium Hyaluronate under Physiological Conditions. *Biomacromolecules*, 2 (1), 65-69.

Koos, M.R.M., Kummerlöwe, G., Kaltschnee, L., Thiele, C.M., Luy. B. (2016). CLIP- COSY: A Clean In- Phase Experiment for the Rapid Acquisition of COSY- type Correlations, *Angewandte Chemie International Edition*, 55, 7655-7659

Mao Che L., Andrefouet S., Bothorel V., Guezennec M., Rougeaux H. & J.Guezennec (2001). Physical, chemical and microbiological characteristics of microbial mats (Kopara) in the south pacific atolls of French Polynesia. *Canadian Journal of Microbiology* 47(11), 994-1012.

Mendichi R, Šoltés, L. & Giacometti Schieroni, A. (2003). Evaluation of radius of gyration and intrinsic viscosity molar mass dependence and stiffness of hyaluronan. *Biomacromolecules* 4(6), 1805-10.

Milas, M., Roure, I., & Berry, G. C. (1996). Crossover behavior in the viscosity of semiflexible polymers: Solutions of sodium hyaluronate as a function of concentration, molecular weight, and temperature. *Journal of Rheology*, 40(6), 1155-1166.

Mo, Y., Takaya, T., Nishinari, K., Kubota, K., & Okamoto, A. (1999). Effects of sodium chloride, guanidine hydrochloride, and sucrose on the viscoelastic properties of sodium hyaluronate solutions. *Biopolymers*, 50(1), 23-34.

Morris, E. R., Rees, D. A., & Welsh, E. J. (1980). Conformation and dynamic interactions in hyaluronate solutions. *Journal of Molecular Biology*, 138(2), 383-400.

Nwodo, U. U.; Green, E.; Okoh, I. A., (2012). Bacterial Exopolysaccharides: Functionality and Prospects. International Journal of Molecular Sciences, 13 (11), 14002-14015.

Nunes, C., Silva, L., Fernandes, A. P., Guiné, R. P. F., Domingues, M. R. M., & Coimbra, M. A. (2012). Occurrence of cellobiose residues directly linked to galacturonic acid in pectic polysaccharides. *Carbohydrate Polymers*, 87(1), 620–626.

Ouwerx C., Velings, N., Mestdagh, M.M., Axelos M.A.V. Physico-chemical properties and rheology of alginate gel beads formed with various divalent cations. *Polymer Gels and Networks*, 6 (1998), 393-408.

Poli A., Anzelmo G. & Nicolaus B (2010) Bacterial exopolysaccharides from extreme marine habitats: production, characterization and biological activities. *Marine Drugs*, 8(6): 1779-1802

Raguénès G, Christen R, Guezennec J., Pignet P and G Barbier (1997). *Vibrio diabolicus* sp.nov., a new polysaccharide-secreting organism isolated from a deep-sea vent polychaete annelid, *Alvinella pompejana*. *International Journal of Systematic and Evolutionary Microbiology*, 47, 989-995.

Rederstorff, E., Weiss, P., Sourice, S., Pilet, P., Xie, F., Sinquin, C., Colliec-Jouault, S. Guicheux, J. & Laïb, S. (2011). An in vitro study of two GAG-like marine polysaccharides incorporated into injectable hydrogels for bone and cartilage tissue engineering. *Acta Biomaterialia*, 7(5), 2119-2130.

Rougeaux H, Kervarec N, Pichon R & Guezennec J. (1999). Structure of the exopolysaccharide of *Vibrio diabolicus* isolated from a deep-sea hydrothermal vent. *Carbohydrate Research*, 322: 40-45.

Rigouin, C., Delbarre-Ladrat, C., Ratiskol, J., Sinquin, C.; Colliec-Jouault, S. & Dion, M., Screening of enzymatic activities for the depolymerisation of the marine bacterial exopolysaccharide HE800. *Applied Microbiology and Biotechnology* 2012, 96 (1), 143-151.)

Senni, K.; Pereira, J.; Gueniche, F.; Delbarre-Ladrat, C.; Sinquin, C.; Ratiskol, J.; Godeau, G.; Fischer, A.-M.; Helley, D.; Colliec-Jouault, S., (2011), Marine Polysaccharides: A Source of Bioactive Molecules for Cell Therapy and Tissue Engineering. *Marine Drugs*, 9 (9).

Senni, K., Gueniche F., Changotade S., Septier D., Sinquin C., Ratiskol J, Lutomski D., Godeau G, Guezennec J., Colliec-Jouault S. (2013). Unusual Glycosaminoglycans from a Deep Sea Hydrothermal Bacterium Improve Fibrillar Collagen Structuring and Fibroblast Activities in Engineered Connective Tissues. *Marine Drugs*, 11(4), 1351.

Selyanin, M. A., Boykov, P. Y., Khabarov, V. N., & Polyak, F. (2015). The History of Hyaluronic Acid Discovery, Foundational Research and Initial Use. In Hyaluronic Acid (pp. 1-8): John Wiley & Sons, Ltd

Shukla, PJ., Nathani, N M. and Dave B. P. (2017). Marine bacterial exopolysaccharides [EPSs] from extreme environments and their biotechnological applications. *International Journal of Research in BioSciences* 6 (4), 20-32

Smidsrød O. and Gudmund. S. (1990). Alginate as immobilization matrix for cells. *Trends in Biotechnology*, 8, 71-78

Takahashi, R., Kubota, K., Kawada, M., & Okamoto, A. (1999). Effect of molecular weight distribution on the solution properties of sodium hyaluronate in 0.2M NaCl solution. *Biopolymers*, 50(1), 87-98.

Viel, S.; Capitani, D.; Mannina, L.; Segre, A. (2003). Diffusion-Ordered NMR Spectroscopy: A Versatile Tool for the Molecular Weight Determination of Uncharged Polysaccharides. *Biomacromolecules*, 4 (6), 1843-1847.

Wang, J.; Salem, D. R.; Sani, R. K. (2019). Extremophilic exopolysaccharides: A review and new perspectives on engineering strategies and applications. Carbohydrate Polymers, 205, 8-26.

Wang, X., Zhang, L., Wu, J., Xu, W., Wang, X., & Lü, X. (2017). Improvement of simultaneous determination of neutral monosaccharides and uronic acids by gas chromatography. *Food Chemistry*, 220, 198-207.

Yanaki, T., & Yamaguchi, T. (1990). Temporary network formation of hyaluronate under a physiological condition. 1. Molecular-weight dependence. *Biopolymers*, 30(3-4), 415-425.

Zanchetta Ph, Lagarde M and Guézennec J (2003a). A new bone-healing material: A hyaluronic acid-like bacterial exopolysaccharide. *Calcified Tissue International*, 72: 74-79

Zanchetta P, Lagarde N and Guézennec J (2003b). Systematic effects on bone healing of a new hyaluronic acid-like bacterial exopolysaccharide. *Calcified Tissue International*, 73: 232-236

Zhang, X.; Lin, H.; Wang, X.; Austin, B., (2018). Significance of Vibrio species in the marine organic carbon cycle—A review. *Science China Earth Sciences*, 61 (10), 1357-1368.

Zykwinska, A., Marquis, M., Sinquin, C., Cuenot, S., & Colliec-Jouault, S. (2016). Assembly of HE800 exopolysaccharide produced by a deep-sea hydrothermal bacterium into microgels for protein delivery applications. *Carbohydrate Polymers*, 142, 213-221.

Table 1. Monosaccharides composition of the sample MO 245 (mg/g).

Monosaccharide	**Rha**[1,2]	**Man**[1]	**Gal**[1]	**Glc**[1]	**GlcA**[2]	**GalA**[2]	**GlcN**[3]	**GalN**[3]
Concentration (mg/g)	vt.	0.3±0.0	3.7±0.0	20.2±13.3	507.3±59.8	n.d.	172.8±2.4	172.6±3.3

[1]The results presented correspond to hydrolysis with 2 M TFA, n=2.[2]The results presented correspond to hydrolysis with 1 M H_2SO_4, n=3. [3]The results presented correspond to hydrolysis with 6 M HCl, n=2. n.d.-not detected; vt.-vestigial.

Table 2 Experimental ^{1}H and ^{13}C NMR chemical shifts (δ, ppm) of MO245 exopolysaccharide. The data was measured at 60 ºC and are referenced to TSP.

Residue	**Experimental Chemical shifts (ppm)**						
	H1	**H2**	**H3**	**H4**	**H5**	**H6**	**Hacetyl**
	C1	**C2**	**C3**	**C4**	**C5**	**C6**	**Cacetyl/C=O**
c, →β-GlcpA(1→	4.66	3.46	3.61	3.68	3.82	--	--
	105.0	74.9	76.4	83.0	77.0	176.8	--
a →α-GalpNAc(1→3)	5.40	4.25	3.87	4.21	3.83	3.74,3.93	2.06
	99.1	52.0	69.8	78.2	72.1	62.3	24.7 /176.2
d, →β-GlcpNAc(1→4)	4.59	3.77	3.70	3.66	3.45	3.65,3.82	2.06
	102.1	55.9	80.2	72.8	77.6	62.5	24.2 /176.7
e, →β-GlcpA(1→	4.52	3.37	3.59	3.77	3.78	--	--
	104.7	75.0	75.4	81.5	78.4	176.9	--

Table 3. Mw (MALS and RALS, kDA) intrinsic viscosity ([η], dl/g)), scaling exponents $[\eta] \sim Mw^{\alpha}$ and $RG \sim Mw^{v}$, radius of gyration (R_g, nm) and hydrodynamic radius (R_h nm) of the MO245 EPS.

	Mw(PDI), RALS[a]	**Mw(PDI), MALS[b]**	$[\eta]$	α [a]	**V[b]**	$Rg_{z,\mathrm{MALS}}$ [b]	$R_{h,\mathrm{DLS}}$[b]
MO245	536±11(1.19±0.02)	513±4 (1.42±0.01)	6.7±0.3	0.81±0.03	0.70±0.02	56±0.3	42±2
HA	--	---	12[c], 13[d]	0.8[e]	0.6[e]	60[c], 93[d],98[f]	35[c], 50[d]

[a] Measured in phosphate buffer, pH 6.7. Mean value of 3 measurements and standard deviation
[b] Measured in PBS buffer pH 7.4. Mean value of 6 measurements and standard deviation
[c] Data taken for comparison purposes from HA Mw 610 kDa (Esquenet & Buhler, 2002)
[d] Data taken for comparison purposes from HA Mw 622 kDa (Takahashi, Kubota, Kawada, & Okamoto, 1999)
[e] Normal value found in the literature for HA (Cowman, & Matsuoka, 2005)
[f] Data taken for comparison purposes from Mw 665 kDa (Mendichi, Šoltés & Giacometti Schieroni, 2003)